Licoricidin Abrogates T-Cell Activation by Modulating PTPN1 Activity and Attenuates Atopic Dermatitis In Vivo

Hyun-Su Lee[1,2], Jooyoung Kim[3], Hyun Gyu Choi[4], Eun-Kyung Kim[5,6] and Chang-Duk Jun[1,2]

Licoricidin, the fifth-highest fraction among the isolated 48 molecules from *Glycyrrhiza uralensis* extracts, has been known as an anti-inflammatory bioactive molecule; however, few studies have shown its inhibitory effect on T-cell activation and atopic dermatitis (AD). This study examined the therapeutic potential of licoricidin in AD by modulating T-cell activation with molecular mechanisms. Licoricidin attenuated the expression of *IL-2* mRNA in stimulated T cells without cytotoxicity. Because tyrosine-protein phosphatase nonreceptor type 1 was predicted to interact physically with licoricidin in T cells in silico analysis, the results of tyrosine-protein phosphatase nonreceptor type 1 activity assay and phosphorylation study predicted that licoricidin might abrogate the activity of tyrosine-protein phosphatase nonreceptor type 1 during T-cell activation. Pretreatment with licoricidin controlled the dephosphorylation of Lck on TCR-mediated stimulation. Moreover, licoricidin alleviated the symptoms of dinitrochlorobenzene- and/or mite extract-induced AD, including ear thickness and serum IgE level. Microscopic analysis also showed the effects of licoricidin on the thickness of the dermis and epidermis and infiltration of immune cells. Furthermore, mRNA levels of proinflammatory cytokines were attenuated in the ear lesions of licoricidin-treated AD mice. Therefore, licoricidin has therapeutic potential for treating AD, and its underlying mechanism involves effective modulation of T-cell activation by controlling tyrosine-protein phosphatase nonreceptor type 1 to maintain Lck phosphorylation.

Journal of Investigative Dermatology (2021) **141,** 2490–2498; doi:10.1016/j.jid.2021.02.759

INTRODUCTION

Atopic dermatitis (AD) is one of the most common immune-related skin diseases caused by immune system imbalance, genetic defects, and environmental influence (Grammatikos, 2008). T-cell activation and differentiation are required for the development of AD symptoms (Brandt and Sivaprasad, 2011). After recognition of allergen presented by Langerhans cells in the skin, naïve T cells are primed by the Langerhans cells. In the T helper (Th)2 cytokines milieu, T cells can be differentiated into Th2 cells that produce IL-4, IL-5, IL-13, and IL-31 (Leung and Bieber, 2003; Oyoshi et al., 2009). Because TCR-mediated stimulation is necessary for T-cell differentiation into effector T cells, regulation of T-cell activation by negative regulators and investigation of the underlying mechanism can be the first step to conquer AD disease.

Tyrosine-protein phosphatase nonreceptor type 1 (PTPN1) is a nonreceptor tyrosine phosphatase and has various substrates that are involved in fundamental cellular functions (Mertins et al., 2008). Therefore, PTPN1 has been studied as a therapeutic target of a wide range of diseases, including diabetes, obesity, and liver disease. Especially, pharmacological inhibition of PTPN1 is widely used for controlling disease development (Agham et al., 2012; Clark et al., 2001; Eichhorst et al., 2004; Krishnan et al., 2015; Zhang and Lee, 2003). However, the studies investigating PTPN1 as a target of immunological diseases involved in T-cell activation have not been reported.

Licorice (*Glycyrrhiza uralensis*) root is traditionally known to be anti-inflammatory in oriental medicine (Zhang et al., 2012). Among hundreds of compounds, glycyrrhizin, liquiritin, and liquiritigenin are widely known as the constituent compounds of licorice (Fu et al., 2005) and are reported to have anti-inflammatory effects (Akamatsu et al., 1991; Kim et al., 2008; Seo et al., 2011). Licoricidin is also a component of licorice and has been reported to reduce the production of bacterial volatile sulfur compounds (Tanabe et al., 2012), attenuate periodontitis diseases by modulating matrix metalloproteinase and cytokine production (La et al., 2011), and exert antibacterial effects against *Staphylococcus aureus* and *Helicobacter pylori* (Fukai et al., 2002; Hatano et al., 2005). However, interestingly, no preceding studies have reported whether licoricidin possesses direct immunomodulating activity.

Therefore, the aim of this study was to investigate whether licoricidin modulates T-cell activation and concurrent inflammation to control AD symptoms in mice.

[1]*School of Life Sciences, Gwangju Institute of Science and Technology (GIST), Gwangju, Republic of Korea;* [2]*Immune Synapse and Cell Therapy Research Center, Gwangju Institute of Science and Technology (GIST), Gwangju, Republic of Korea;* [3]*Office of Academic Affairs, Konkuk University, Chungju, Republic of Korea;* [4]*College of Pharmacy, Research Institute of Pharmaceutical Sciences, Kyungpook National University, Daegu, Republic of Korea;* [5]*Department of Food Science and Nutrition, College of Health Sciences, Dong-A University, Busan, Republic of Korea; and* [6]*Center for Silver-targeted Biomaterials, Brain Busan 21 Plus program, Dong-A University, Busan, Republic of Korea*

Correspondence: Eun-Kyung Kim, Department of Food Science and Nutrition, College of Health Sciences, Dong-A University, Busan 49315, Republic of Korea. E-mail: ekkim@dau.ac.kr

Abbreviations: AD, atopic dermatitis; DC, dendritic cell; dLN, draining lymph node; DNCB, dinitrochlorobenzene; PTPN1, tyrosine-protein phosphatase nonreceptor type 1; S50, serine 50 amino acid; siRNA, single interfering RNA; Th, T helper

Received 9 July 2020; revised 13 January 2021; accepted 16 February 2021; accepted manuscript published online 20 April 2021; corrected proof published online 14 August 2021

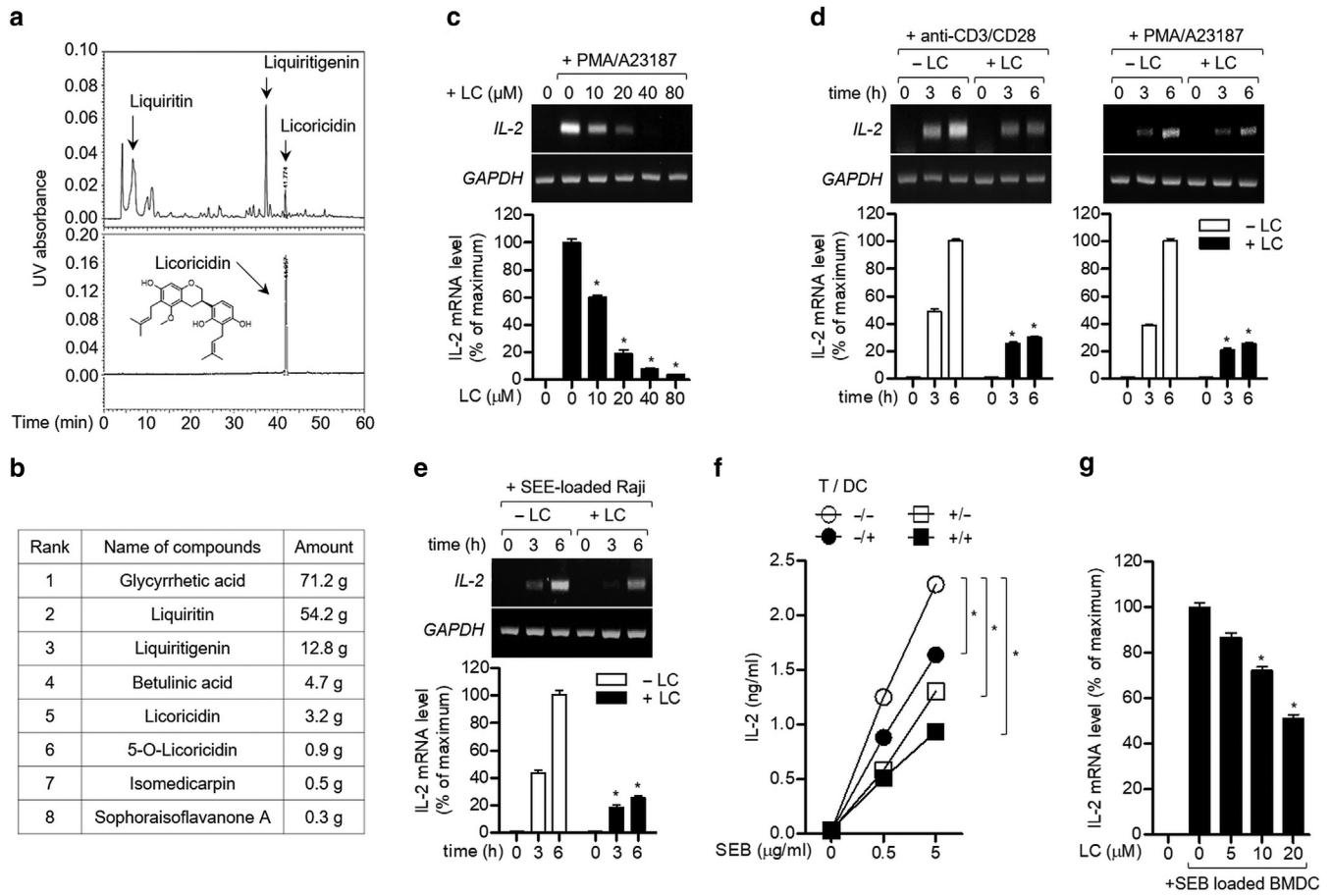

Rank	Name of compounds	Amount
1	Glycyrrhetic acid	71.2 g
2	Liquiritin	54.2 g
3	Liquiritigenin	12.8 g
4	Betulinic acid	4.7 g
5	Licoricidin	3.2 g
6	5-O-Licoricidin	0.9 g
7	Isomedicarpin	0.5 g
8	Sophoraisoflavanone A	0.3 g

Figure 1. Licoricidin isolated from *Glycyrrhiza uralensis* inhibits IL-2 production in activated T cells. (**a**) Isolated licoricidin from *G. uralensis* was identified by HPLC and its chemical structure. (**b**) List of the amount of isolated constituents from 6 kg of *G. uralensis*. (**c**–**e**) mRNA levels of *IL-2* from activated Jurkat T cells pretreated with the indicated concentration of licoricidin. (**f**) Licoricidin-treated mouse $CD4^+$ T cells and mouse BMDCs pulsed with SEB were coincubated for 24 h in a U-bottom 96-well plate. Produced mouse IL-2s were measured by ELISA from the supernatant. (**g**) mRNA levels of *IL-2* from $CD4^+$ T cells cocultured with SEB-pulsed BMDCs were measured. Results are expressed as mean ± SEM of three independent experiments. $*P < 0.05$. BMDC, bone marrow–derived dendritic cell; DC, dendritic cell; h, hour; min, minute; PMA, phorbol 12-myristate 13-acetate; SEB, staphylococcal enterotoxin B; SEE, staphylococcal enterotoxin E.

RESULTS

Licoricidin isolated from *G. uralensis* inhibits IL-2 production in activated T cells

Licoricidin that was the fifth-highest constituent in *G. uralensis* was isolated and used for this study (Figure 1a and b). First, we determined whether licoricidin modulates T-cell function by defining the mRNA level of *IL-2* in the activated condition with licoricidin. Licoricidin dramatically inhibited *IL-2* expression in a dose-dependent manner (Figure 1c). The time-dependent experiment with 20 μM also showed that licoricidin strongly downregulated T-cell activation stimulated by immobilized anti-CD3/-CD28 antibodies and phorbol 12-myristate 13-acetate/A23187 stimulation (Figure 1d). Pretreatment with 20 μM licoricidin also reduced the proliferation of T cells in the presence of TCR-mediated stimulation (Supplementary Figure S1a). Furthermore, it was examined whether licoricidin negatively modulates T-cell activation in conjugation with antigen-loaded antigen-presenting cells. Jurkat T cells pretreated with 20 μM of licoricidin and cocultured with staphylococcal enterotoxin E-pulsed B cells in a time-dependent manner revealed a declined mRNA level of *IL-2* (Figure 1e). Pretreatment of T cells and dendritic cells (DCs) with licoricidin separately showed a negative effect on T-cell activation (Figure 1f). Dose-dependent pretreatment with licoricidin also reduced *IL-2* production from stimulated mouse T cells by coculture with staphylococcal enterotoxin B–pulsed bone marrow–derived DCs (Figure 1g). These data suggest that licoricidin has profound inhibitory effects on T-cell functions in stimulated conditions.

Licoricidin does not influence cytotoxicity in T cells

Because cytotoxicity can be a critical mechanism of immunosuppression on T cells, we tested the cytotoxicity of licoricidin on T cells using Jurkat T-cell line and mouse primary $CD4^+$ T cells. As shown in Figure 2a and Supplementary Figure S2a, treatment with licoricidin up to 40 μM did not show a cytotoxic effect to both human T-cell line and mouse primary T cells, but 80 μM licoricidin induced cell death from the result of MTT assay. Cellular confluency was consistent with MTT assay result that treatment with only 80 μM licoricidin reduces the confluency of Jurkat cells (Figure 2b). In particular, experimental results from AnnexinV–propidium iodide apoptosis assay (Figure 2c and Supplementary Figure S2b) and detected AnnexinV expression by IncuCyte (Supplementary Figure S2c) confirmed that treatment with only 80 μM licoricidin leads to the cellular apoptosis.

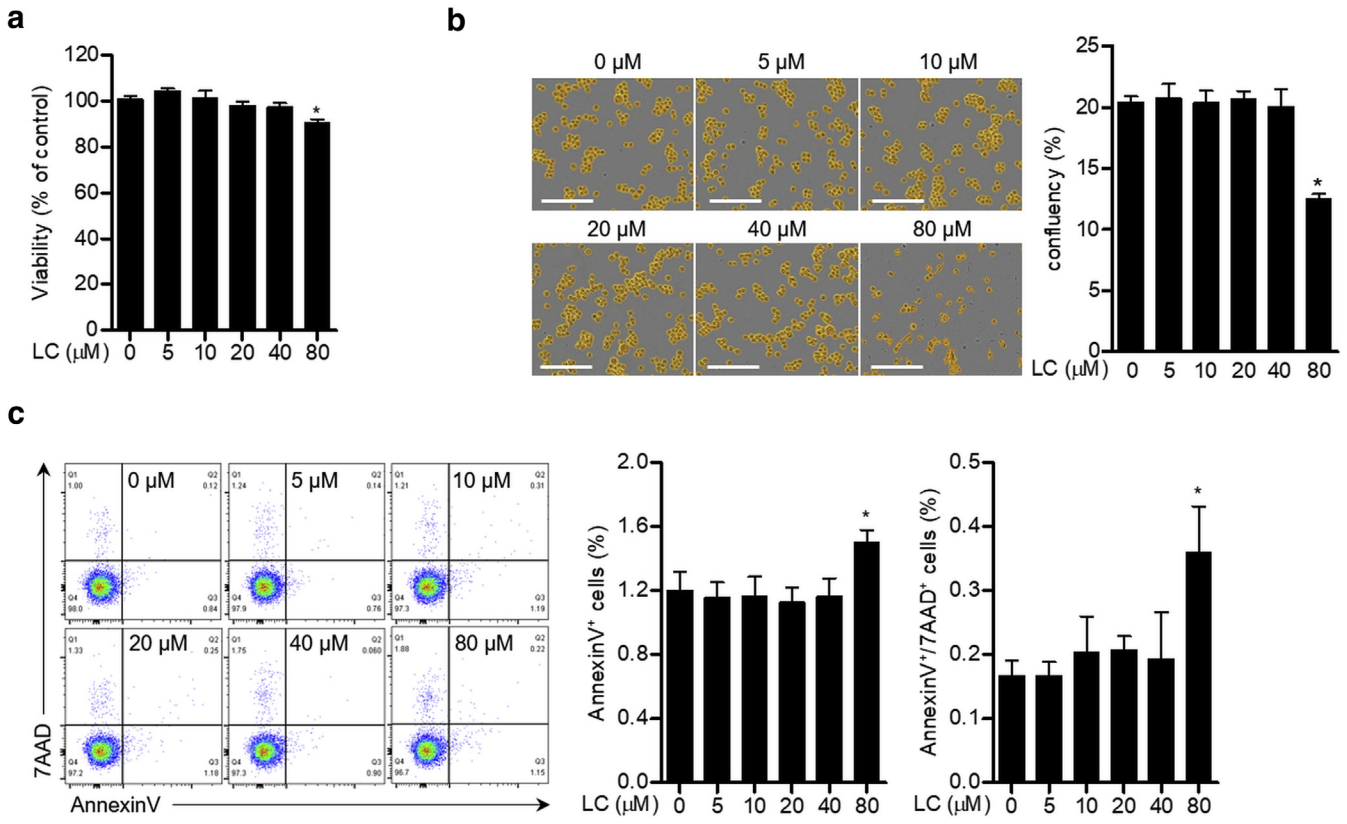

Figure 2. Licoricidin does not influence cytotoxicity in T cells. (**a**) Cell viability was measured by MTT assay after incubation of the indicated concentration of licoricidin for 24 h. (**b**) Jurkat T cells were treated with the indicated concentration of licoricidin for 24 h, and cellular confluency was assessed by IncuCyte imaging system. (**c**) Jurkat T cells were treated with the indicated concentration of licoricidin for 24 h, and apoptotic and necrotic cells were quantified by AnnexinV–7-AAD assay. Results are expressed as mean ± SEM of three independent experiments (*$P < 0.05$). Bar = 0.2 mm. 7-AAD, 7-aminoactinomycin D; h, hour.

PTPN1 is a target of licoricidin in activated T cells

To uncover the molecular mechanism underlying the bioactivity of licoricidin in T cells, the target proteins of licoricidin were investigated using online servers for small-molecule target prediction. As shown in Supplementary Table S1, tyrosine-protein phosphatase type 1 (gene code *PTPN1*) was predicted as the potential target of licoricidin by Swiss TargetPrediction, a publicly available webserver to predict the targets for novel small bioactive molecules. Consistently, Because previous publication has shown that PTPN1 plays a key role in DC maturation, DC migration, and T-cell activation, this in silico data led us to consider that PTPN1 can be a target of licoricidin (Martin-Granados et al., 2015). PTPN1 activity assay assured that licoricidin lessens PTPN1 activity in a dose-dependent manner (Figure 3a). The phosphorylation of serine 50 amino acid (S50) has been studied and has been shown to be a critical step in the protein kinase B–mediated inactivity of PTPN (Ravichandran et al., 2001). Therefore, the phosphorylation of the S50 site in Jurkat cells after TCR-mediated stimulation was analyzed to investigate whether licoricidin affects the inactivity of PTPN1. As shown in Figure 3b, the phosphorylation of the S50 site of PTPN1 was increased in Jurkat cells treated with licoricidin compared with that in the mock-treated Jurkat cells. A knockdown study of PTPN1 by RNA interference also indicated that these T cells showed significantly reduced *IL-2* mRNA levels and proliferation and IL-2 production after TCR-mediated stimulation and phorbol 12-myristate 13-acetate/A23187 stimulation without any cytotoxicity (Figure 3c and d and Supplementary Figure S3). In parallel, structure docking prediction showed that licoricidin localized with the catalytic domain of PTPN1 consistent with Ertiprotafib, which is the inhibitor of PTPN1 (Figure 3e). Supplementary experiment results in DCs also showed that pretreatment with licoricidin regulates DC maturation and function, which are highly associated with PTPN1 activity, and they showed that licoricidin acts as an antagonist of PTPN1 in other immune cells (Supplementary Figure S4). Accordingly, these data assume that licoricidin regulates the activity of PTPN1 by regulating the phosphorylation of the S50 site of PTPN1 and that PTPN1 is a potential target of licoricidin in T-cell activation.

Licoricidin phosphorylates Lck by regulating PTPN1 activity on T-cell activation

In the TCR-mediated stimulation pathway, dephosphorylation of Lck by CD45 is mostly the initial step for T-cell activation (Mustelin et al., 1989). Because the SH3 domain of Lck is localized within the catalytic domain of PTPN1, one of the CD45 family (He et al., 2014), where licoricidin localizes in T cells (Figure 4a), we decided to examine whether licoricidin directly regulates the dephosphorylation of Lck (Y505 site) after TCR-engaged stimulation. Licoricidin-treated Jurkat cells showed a significantly comparable level of phosphorylated Lck Y505 and promoted the phosphorylation of PTPN1

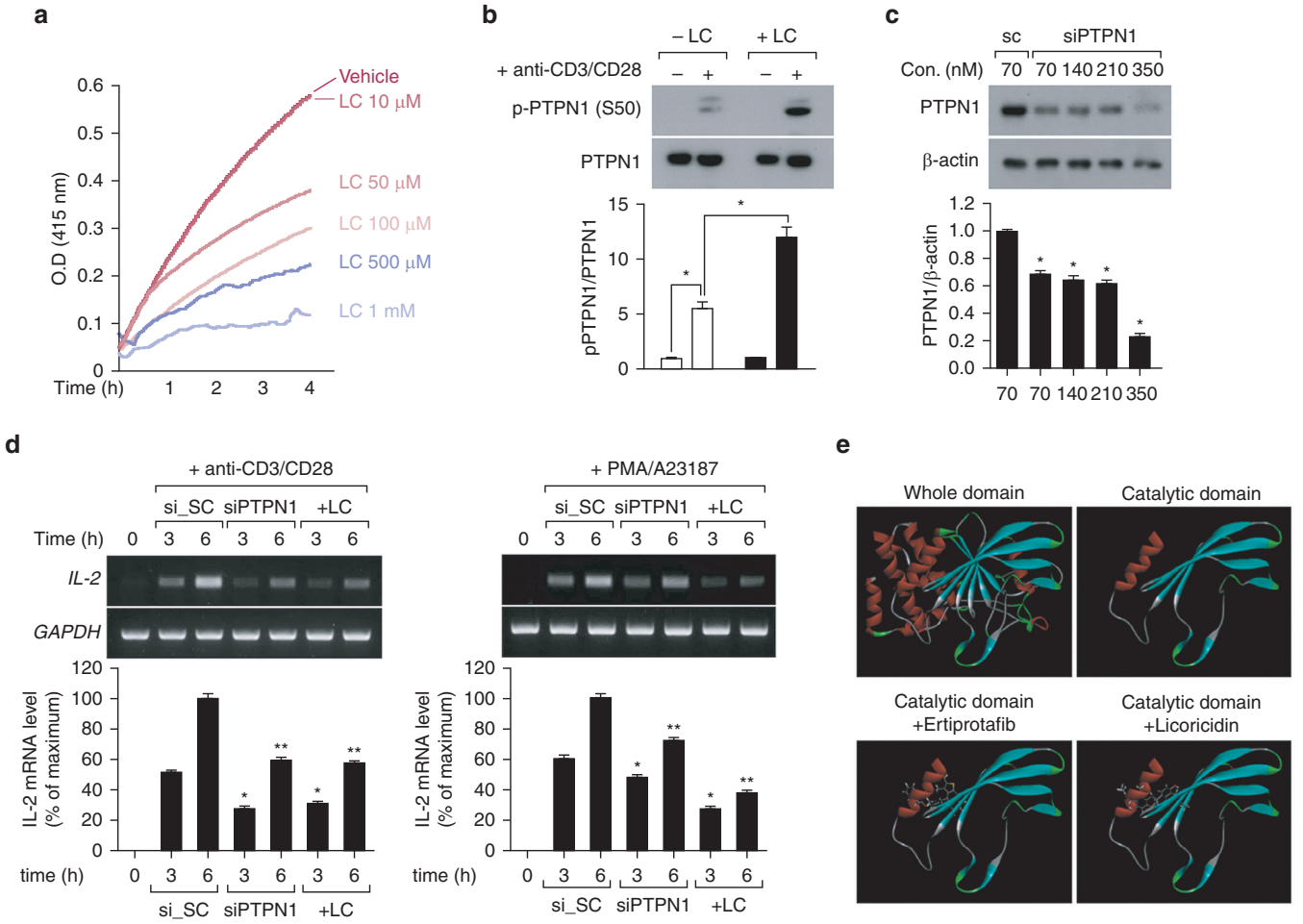

Figure 3. PTPN1 is a target of licoricidin in activated T cells. (**a**) The result of PTPN1 activity assay with treatment with the indicated concentration of licoricidin. (**b**) Phosphorylated PTPN1 (S50) was detected by western blot from activated Jurkat T cells pretreated with 20 μM licoricidin. (**c**, **d**) The expression of PTPN1 was determined by western blot assay from Jurkat cells transfected with indicated concentrations of (**c**) si_SC or si_PTPN1, and *IL-2* mRNA levels were detected from Jurkat T cells transfected or treated with (**d**) licoricidin. (**e**) A predicted model showing the interaction of Ertiprotafib with the catalytic domain of PTPN1 and licoricidin with the catalytic domain of PTPN1 generated using DSV software. Results are expressed as mean ± SEM of three independent experiments. $*P < 0.05$, $**P < 0.01$. Con., concentration; h, hour; O.D, optical density; PMA, phorbol 12-myristate 13-acetate; p-PTPN1, phosphorylated tyrosine-protein phosphatase nonreceptor type 1; PTPN1, tyrosine-protein phosphatase nonreceptor type 1; S50, serine 50 amino acid; SC, scrambled;;si_PTPN1, small interfering tyrosine-protein phosphatase nonreceptor type 1; si_SC, small interfering scrambled.

at S50 compared with that in the mock-treated Jurkat cells in a dose- (Figure 4b) and time-dependent experiment (Figure 4c). Interestingly, the down signaling molecules of Lck, including ZAP70, LAT, protein kinase C gamma 1, and extracellular signal–regulated kinase, were decreased in licoricidin-treated Jurkat cells (Figure 4d). Furthermore, the levels of phosphorylated Lck in Jurkat cells transfected with PTPN1 single interfering RNA (siRNA) were equivalent to the level of phosphorylated Lck in resting Jurkat cells; however, phosphorylation of ZAP70 and extracellular signal–regulated kinase after TCR-engaged stimulation was remarkably decreased (Figure 4e). These data show that licoricidin inhibits the dephosphorylation of Lck by modulating PTPN1 activity and attenuates the phosphorylation of signal transduction molecules in TCR-mediated activation.

Licoricidin effectively attenuates AD symptom in vivo

Because numerous studies have shown that T cells play a pivotal role in the development and maintenance of the pathogenesis of AD (Akdis et al., 2002; Santamaria Babi et al., 1995), we further verified that licoricidin has potential as a modulator for AD with dinitrochlorobenzene (DNCB) and house dust mite extract to the ears by oral administration of licoricidin for 28 days (Figure 5a). As shown in Figure 5b and c, licoricidin-treated AD mice showed dramatically attenuated symptoms. Because the skin lesions associated with AD have archetypal microscopic characteristics, including hyperkeratosis, parakeratosis, acanthosis, and infiltration of immune cells, we investigated the skin manifestations in AD mice and licoricidin-treated AD mice microscopically (Figure 5d). H&E staining revealed that the epidermal and dermal tissues in licoricidin-treated AD mice were significantly thinner than those in AD mice (Figure 5e), and toluidine blue staining of licoricidin-treated AD mice ear tissue sections exhibited a remarkably decreased number of infiltrated master cells (Figure 5f). Next, the IgE levels in AD mice were measured because increased IgE production is the main event and induces various atopic pathogenesis, including AD (Liu et al., 2011). As expected, licoricidin-treated AD mice produced dramatically lesser IgE and mite-

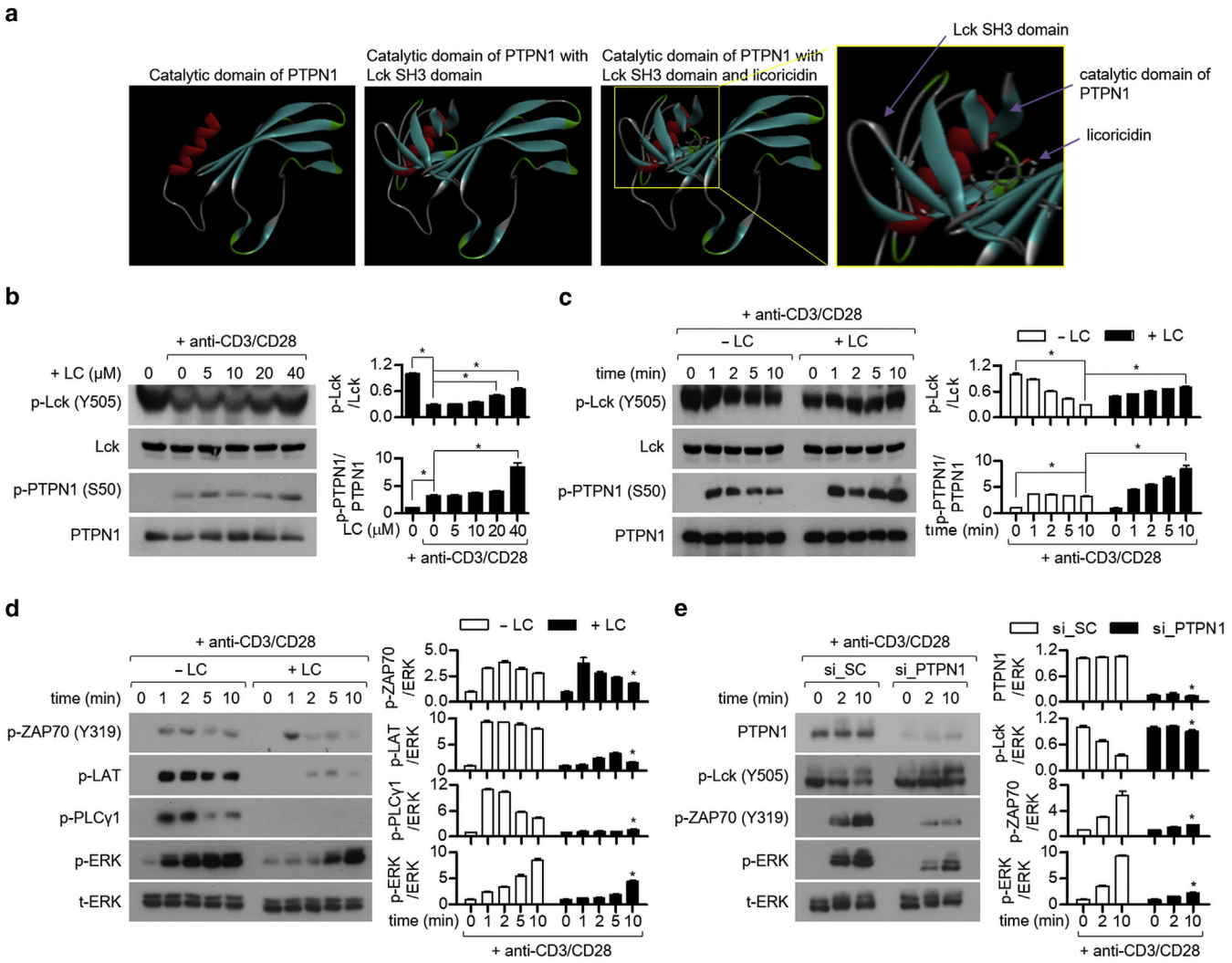

Figure 4. Licoricidin maintains Lck phosphorylation by regulating PTPN1 activity in T-cell activation. (**a**) A predicted model depicting the catalytic domain of PTPN1 (left), the catalytic domain of PTPN1 with Lck SH3 domain (middle), and licoricidin with Lck SH3 domain (right) generated using DSV software. (**b–d**) The expression of the indicated proteins was measured by western blot from Jurkat T cells pretreated with the indicated concentrations of licoricidin and stimulated for the indicated time. (**e**) Transfected Jurkat cells were activated for the indicated time, and the amounts of the indicated proteins were measured by western blot. Results are expressed as mean ± SEM of three independent experiments. $*P < 0.05$. ERK, extracellular signal–reguated kinase; min, minute; p-ERK, phosphorylated extracellular signal–reguated kinase; p-LAT, phosphorylated LAT; p-Lck, phosphorylated Lck; p-PLCγ1, phosphorylated protein kinase C gamma 1; p-PTPN1, phosphorylated tyrosine-protein phosphatase nonreceptor type 1; PTPN1, tyrosine-protein phosphatase nonreceptor type 1; p-ZAP70, phosphorylated ZAP70; S50, serine 50 amino acid; si_PTPN1, small interfering tyrosine-protein phosphatase nonreceptor type 1; si_SC, small interfering scrambled; t-ERK, total extracellular signal–reguated kinase.

specific IgE than AD control mice on day 28 (Figure 5g). To exhibit the alteration of gene expressions of pathogenic cytokines, real-time quantitative PCR analysis was performed from the removed ear tissues. As shown in Figure 5h, mRNA levels of *IL-4*, *IL-5*, *IL-6,* and *IL-13* were dramatically declined in licoricidin-treated AD mice. Results from T-cell differentiation assay in vitro also showed that licoricidin regulates Th1 and Th2 differentiation (Supplementary Figure S5). These data suggest that licoricidin attenuates AD symptoms in a mice model and imply that licoricidin might be an adequate modulator of immune responses in AD.

Oral administration of licoricidin diminished the systemic AD manifestations and mRNA level of inflammatory cytokines in the ear tissue

Systemic AD manifestations are discovered after induction of AD by DNCB and mite extracts in previous studies (Lee et al., 2016, 2015). Among the systemic AD manifestations, increased size of draining lymph nodes (dLNs) was observed in AD mice; however, licoricidin-treated AD mice showed lesser size and weight of dLNs than AD mice (Figure 6a). To find the correlation between swelled lymph nodes and infiltrating T cells into lymph nodes, immunocytochemical analysis in the tissue section was performed. Immunocytochemical analysis showed that the infiltration of Th cells into the lymph nodes was remarkably diminished in AD mice with licoricidin administration compared with that in AD control mice (Figure 6b). We further explored the levels of inflammatory cytokines, which are involved in the pathogenesis of AD, in the dLNs to determine whether licoricidin has regulatory effects on Th2 cells. As shown in Figure 6c, licoricidin-treated AD mice downregulated the levels of cytokines, including IL-2, IL-4, IL-5, and IL-13, which are generally known as Th2 cytokines. Besides, the expression of

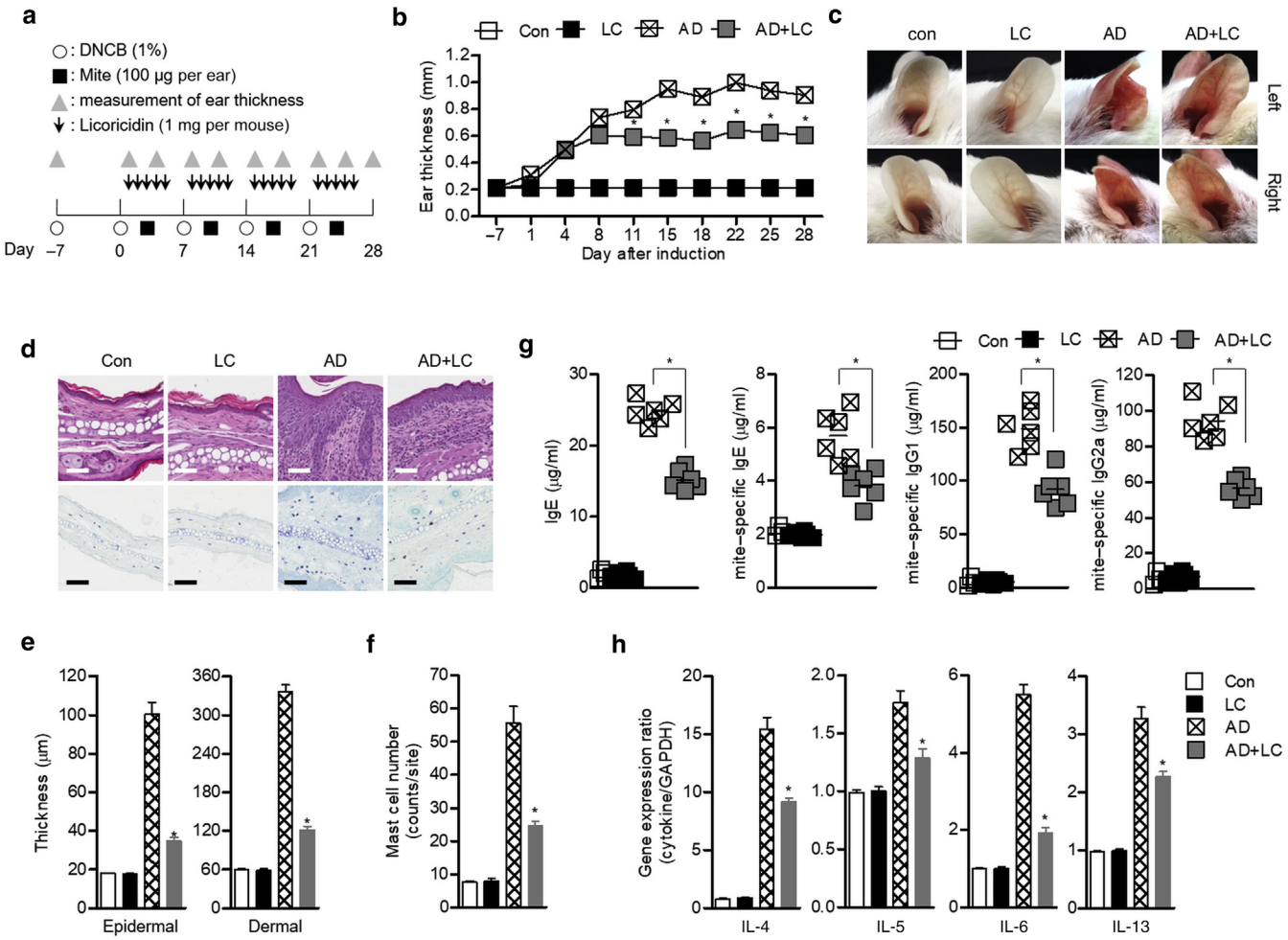

Figure 5. Licoricidin effectively attenuates AD symptoms in vivo. (**a**) Experimental scheme of AD. (**b**) Ear thickness changes in 28 days. (**c**) Representative pictures of mice ears on day 28. (**d**) Microscopic pictures of the ear sections stained with H&E (×200, upper) and toluidine blue (×100, bottom); white bar = 100 μm, black bar = 200 μm. (**e**) Epidermal and dermal thickness was measured from the ear sections in **d**. (**f**) Infiltrating mast cells were counted from the ear section in **d**. (**g**) Serum IgE, mite-specific IgE, IgG1, and IgG2a levels measured by ELISA. (**h**) mRNA levels of cytokines in the ear tissues. Data are expressed as the mean ± SEM (n = 6 per group). *$P < 0.05$. Con indicates the control mice, LC indicates the mice receiving licoricidin AD indicates the mice with AD, and AD+LC indicates the mice with AD receiving licoricidin. AD, atopic dermatitis; Con, control; DCNB, dinitrochlorobenzene.

GATA3 in $CD4^+$ T cells from dLNs of licoricidin-treated AD mice was significantly abrogated compared with that in AD control mice (Figure 6d). To confirm whether the oral administration of licoricidin affects the activity of PTPN1 in vivo, we checked the phosphorylation level of Lck and PTPN1 at S50 on $CD4^+$ T cells isolated from dLNs. Figure 6e shows that the oral administration of licoricidin clearly blocked the dephosphorylation of Lck but enhanced the phosphorylation of PTPN1 at S50. These data show that the oral administration of licoricidin systemically affects the AD symptoms regulating the function of T cells infiltrated into the ear tissues by blocking the expression of pathogenic Th2 cytokines and GATA3 by the regulation of PTPN1 activity.

DISCUSSION

It has been reported that phosphorylation of PTPN1 plays different biological roles in cellular mechanisms depending on its sites (Yip et al., 2010). Protein kinase C phosphorylates serine 378, serine 352, and serine 386 sites of PTPN1 depending on the stage of the cell cycle (Flint et al., 1993; Shifrin et al., 1997), Y 66, Y 152, and Y 153 sites could be phosphorylated by stimulation with insulin, and they modulate the association with insulin receptors (Bandyopadhyay et al., 1997). In 2001, it was discovered that phosphorylation at the serine 50 site by protein kinase B can decrease PTPN1 activity and impair its ability to dephosphorylate the insulin receptors in the case of insulin-mediated signaling (Ravichandran et al., 2001). In TCR-engaged stimulation, PTPN1 was phosphorylated at S50, resulting in dissociation of phosphate from Lck (Figures 3b and 4b). However, in licoricidin-treated Jurkat cells, phosphorylation at S50 was elevated, but dephosphorylation of Lck was decreased (Figure 4b and c). This increased phosphorylation of the S50 site by licoricidin could have led to the inactivation of PTPN1 and allowed Lck to maintain the phosphorylated form. This data suggested that licoricidin modulates T-cell activation in TCR-mediated stimulation by augmenting the phosphorylation of the S50 site.

Computational tools for predicting the proteins that interact with small molecules and the score, which presents probability in silico, are widely used to identify target protein of bioactive molecules. By applying structure-based

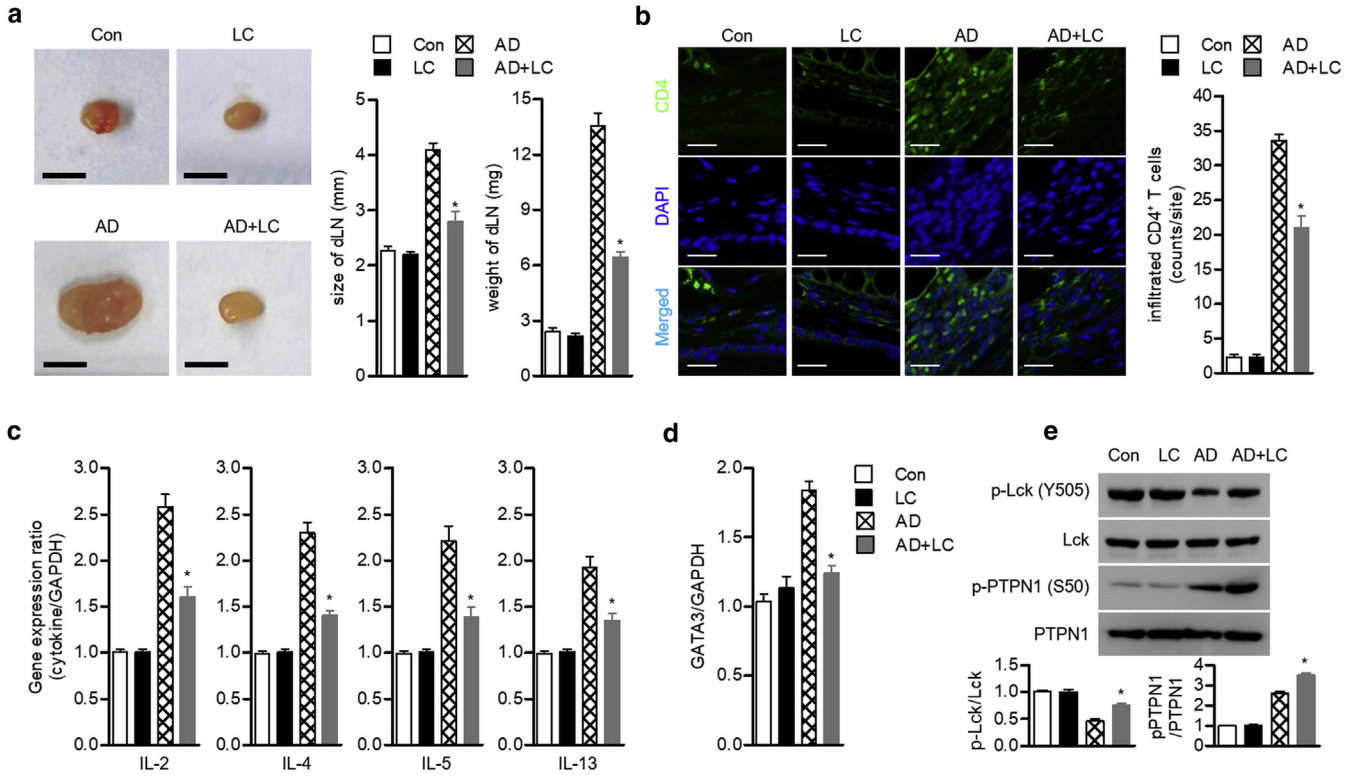

Figure 6. Oral administration of licoricidin diminished the systemic AD manifestations and mRNA level of inflammatory cytokines in the ear tissue. (**a**) Representative pictures of dLNs on day 28 after AD induction (left) and their size (middle) and weight (right). Black bar = 2 mm. (**b**) Photomicrographs of the lymph nodes sections isolated on day 28 after AD induction and stained with an anti-CD4 antibody and DAPI. White bar = 20 μm. (**c**, **d**) Expression of (**c**) cytokines and (**d**) GATA3 in the helper T cells isolated from dLNs were measured by real-time PCR. (**e**) The phosphorylated Lck and PTPN1 at S50 were detected by western blot on the $CD4^+$ T cells isolated from dLNs. Data are expressed as the mean ± SEM (n = 6 per group). *$P < 0.05$. White bar = 20 μm. Con indicates the control mice, LC indicates the mice receiving licoricidin, AD indicates the mice with AD, and AD+LC indicates the mice with AD receiving licoricidin. AD, atopic dermatitis; dLN, draining lymph node; p-Lck, phosphorylated Lck; p-PTPN1, phosphorylated tyrosine-protein phosphatase nonreceptor type 1; PTPN1, tyrosine-protein phosphatase nonreceptor type 1; S50, serine 50 amino acid.

computational approaches, several proteins that play critical roles in T-cell activation, which could be possible targets of licoricidin, were identified. Among these, PTPN1 was identified as a potential target of licoricidin by similarity-based comparison analysis. On the basis of this in silico prediction, activity-based in vitro assays, including cell-based functional assays and loss-of-function study, were performed, and they confirmed that this prediction was worth analyzing. To the best of our knowledge, no previous study has reported that PTPN1 plays a positive role in T-cell activation. It has been shown that tyrosine phosphatase family functions as a positive regulator of T-cell activation. CD45 is the most well-studied molecule in this family and has been known as an essential distal SMAC that acts as a phosphatase on T-cell activation (Altin and Sloan, 1997; Johnson et al., 2000). CD45 is highly involved in T-cell activation through the detachment of one phosphate from Lck. Therefore, it was investigated whether PTPN1 can function as a phosphatase in the dephosphorylation of Lck in the case of T-cell activation. The knockdown of PTPN1 by siRNA in T cells maintained the phosphorylation of Lck (Figure 4e) and abrogated IL-2 production on TCR-mediated stimulation (Figure 3d). Besides, western blotting data showed that licoricidin increased the PTPN1 inactivity by increasing the phosphorylation at S50 (Figure 4b). Taken together, the findings of this study highlight the efficacy of licoricidin in preventing T-cell activation.

MATERIALS AND METHODS

Cell culture

Jurkat T cells (CRL-1651, ATCC, Manassas, VA) and Raji B cells (CCL-86, ATCC) were grown in RPMI medium (Gibco-BRL, Gaithersburg, MD) supplemented with 10% fetal bovine serum, penicillin G (100 units/ml), streptomycin (100 μg/ml), and L-glutamine (2 mM). Mouse $CD4^+$ T cells from the spleen were isolated using magnetic-activated cell sorting separation (magnetic-activated cell sorting, Miltenyi Biotec, Bergisch Gladbach, Germany). Mouse DCs were differentiated from bone marrow using 20 ng/ml of recombinant mouse GM-CSF for 6 days. All cell lines and primary mouse cells were grown at 37 °C in a humidified incubator containing 5% carbon dioxide and 95% air.

Mice

Female BALB/c mice aged 8 weeks were purchased from Samtako (Osan, Republic of Korea) and housed in specific pathogen-free conditions. All experiments were approved by the Animal Care and Use Committee of the School of Life Sciences, Gwangju Institute of Science and Technology, Republic of Korea (approval number: GIST2014-31).

Reagents and antibodies

Anti–human CD3 (OKT3) was purified from hybridoma culture (CRL-8001, ATCC) and antibody to human CD28 was purchased from R&D Systems (Minneapolis, MN). Rabbit anti–phosphorylated Lck, rabbit anti-Lck, rabbit anti–phosphorylated LAT, rabbit anti–phosphorylated protein kinase C gamma 1, rabbit anti–protein kinase C gamma 1, rabbit anti–phosphorylated ZAP70, rabbit anti-ZAP70, rabbit anti–phosphorylated extracellular signal–regulated kinase, and rabbit anti–extracellular signal–regulated kinase were purchased from Cell Signaling Technology (Beverly, MA). Mouse anti–human PTPN1 antibody was obtained from Merck Millipore (Merck, Darmstadt, Germany). Rabbit anti–phosphorylated PTPN1 antibody was obtained from ECM Biosciences (Versailles, KY). Annexin V, 7-aminoactinomycin D, and mouse IgE ELISA kits were purchased from BD Biosciences (San Diego, CA). Phorbol 12-myristate 13-acetate; calcium ionophore (A23187); DAPI; 3-(4, 5-dimethylthiazolyl-2)2, 5-diphenyltetrazolium bromide; tetramethylrhodamine B isothiocyanate–conjugated phalloidin, DNCB, house dust mite extract, and toluidine blue were obtained from Sigma-Aldrich (St. Louis, MO). Staphylococcal enterotoxin B was obtained from Toxin Technology (Sarasota, FL). Rat antibody to mouse CD4 was obtained from BioLegend (San Diego, CA). Recombinant mouse GM-CSF was obtained from Peprotech (Hamburg, Germany). Scrambled siRNA and PTPN1-targeting siRNA were purchased as a pool of four siRNA duplexes from GE Healthcare Dharmacon (Chicago, IL). PTPN1 colorimetric assay kit was acquired from BPS Bioscience (San Diego, CA).

Preparation of licoricidin from the roots of *G. uralensis*

The dried roots (6 kg) were extracted three times with 100% of methanol (10 l × 3) at 70 °C for 3 hours. The filtered extract was concentrated to give a residue (1.2 kg) that was dissolved in water and continuously partitioned with organic solvents (hexanes, methylene chloride, ethyl acetate, and water). The ethyl acetate-soluble extract (70 g) was subjected to chromatography on a silica gel column eluted with a gradient mixture of solvents from 100% methylene chloride to 100% ethyl acetate to obtain seven fractions (Fr. 1-Fr. 7). Fr. 3 (3.2 g), which showed the highest amount of licoricidin, was purified by recrystallization with cold methanol to obtain compound 1 (3.2 g, 0.69% [w/w]). The isolated compound 1 was identified as licoricidin, and it showed >99% purity by HPLC (Figure 1a). Isolated compounds from the extract of *G. uralensis* are listed by obtained amounts in Figure 1b.

T-cell stimulation

Jurkat cells and mouse $CD4^+$ T cells were pretreated with licoricidin at the indicated concentration for 30 minutes at 37 °C. The cells were stimulated with phorbol 12-myristate 13-acetate (100 nM) and A23187 (500 nM) for the indicated times. For TCR-mediated stimulation, the cells were stimulated in the plates containing immobilized anti-CD3 (20 μg/ml) and anti-CD28 (7 μg/ml) for the indicated times. For superantigen stimulation, T cells were incubated with 1 μg/ml staphylococcal enterotoxin E-pulsed Raji B cells or 1 μg/ml staphylococcal enterotoxin B–pulsed mouse bone marrow–derived DCs for the indicated times.

Prediction of the target protein

The candidate target proteins of licoricidin were predicted by the Swiss TargetPrediction server (http://www.swisstargetprediction.ch). The following canonical simplified molecular-input line-entry system code was used for searching: CC(=CCC1=C(C=CC(=C1O)C2CC3=C(C(=C(C=C3OC2)O)CC=C(C)C)OC)O)C. Probabilities were computed on the basis of cross validation. Candidate proteins were cut off by probabilities. Seven candidates were obtained.

Induction of AD in the mice ear

AD in BALB/c mice was induced by repeated topical application of mite extract and DNCB on the ears as described previously (Choi et al., 2013). The experimental protocol used in this study is depicted schematically in Figure 5a. There were four mice groups, namely, healthy control mice that were not treated with either DNCB/mite extract or licoricidin, control mice that were treated with DNCB/mite extract alone or licoricidin alone, and test mice that were treated simultaneously with both DNCB/mite extract and licoricidin. To induce AD, the surfaces of both ear lobes were stripped five times with a surgical tape (Seo-il chemistry, Hwa-sung, Korea). After stripping, each ear was painted with 20 μl of DNCB (1%). Four days later, the ears were painted with 20 μl of mite extract (10 mg/ml). The mite extract/DNCB treatment was repeated weekly for 4 weeks. Licoricidin treatment consisted of oral administration at a concentration of 50 mg/kg/day. The treatment started 1 day after the second DNCB application and was repeated daily for the subsequent 4 days. After a 2-day break, this 5-days-on and 2-days-off licoricidin treatment protocol was repeated for 4 weeks. Ear thickness was measured 24 hours after the application of DNCB or mite extracts using a dial thickness gauge (Kori Seiki MFG, Tokyo, Japan). The mice were killed on day 28.

Histological analysis

After killing the mice their ears were removed and subjected to histopathological analysis. The removed ears were fixed in 10% paraformaldehyde and embedded in paraffin. The paraffin-embedded tissues were sliced into 5-μm-thick sections, deparaffinized, and stained with H&E for measuring the thickness of the epidermis and dermis. To determine the infiltrating mast cells, sliced sections were stained with 0.01% toluidine blue, and the mast cells at three randomly selected sites were counted. To count the infiltrating and apoptotic $CD4^+$ T cells in the ear tissues, the paraffinized blocks were stained with anti-mouse CD4 antibodies overnight. After washing, the slides were stained with rat IgG conjugated with Texas Red for 2 hours. After washing, the slides were stained with TUNEL according to the manufacturer's instructions. The slides were observed under a confocal microscope, and $CD4^+$ T cells were counted at three randomly chosen sites.

Statistics

The mean values were calculated from the data obtained from at least three separate experiments performed on separate days. The unpaired Student's *t*-test and one-way ANOVA were used to identify the significant data. Differences between the groups were considered significant at $P < 0.05$.

Data availability statement

Datasets related to this article can be found at http://www.swisstargetprediction.ch/result.php?job=1827282435&organism=Homo_sapiens, a publicly available online data repository hosted by Swiss Target Prediction (Gfeller et al., 2014).

ORCIDs
Hyun-Su Lee: https://orcid.org/0000-0002-4229-003X
Jooyoung Kim: https://orcid.org/0000-0002-8755-1918
Hyun Gyu Choi: https://orcid.org/0000-0003-0883-4520
Eun-Kyung Kim: https://orcid.org/0000-0002-4832-6427
Chang-Duk Jun: https://orcid.org/0000-0002-1372-9277

CONFLICT OF INTEREST

The authors state no conflict of interest.

ACKNOWLEDGMENTS

This work was supported by the Creative Research Initiative Program(2015R1A3A2066253) through the National Research Foundation grants funded by the Ministry of Science and ICT; by Gwangju Institute of Science and Technology Research Institute IBBR grant funded by the Gwangju Institute of Science and Technology in 2020 and 2021; by the Joint Research Project of Institutes of Science and Technology (2020–2021), Korea; and by the BB21+ Project in 2021. The Basic Science Research Program through the National Research Foundation of Korea (NRF) funded by the Ministry of Education, Science and Technology (NRF-2020R1A2C1014798). EKK and CDJ wrote and equally co-corresponded to finalize the manuscript.

AUTHOR CONTRIBUTIONS

Conceptualization: HSL, CDJ; Data Curation: HSL, JK, HGC; Formal Analysis: HSL; Funding Acquisition: EKK, CDJ; Investigation: HSL, HGC; Methodology: HSL, HGC; Project Administration: EKK; Resources: HGC, CDJ; Software: HSL; Supervision: EKK; Validation: HSL, JK; Visualization: HSL; Writing - Original Draft Preparation: HSL; Writing - Review and Editing; JK, EKK.

SUPPLEMENTARY MATERIAL

Supplementary material is linked to the online version of the paper at www.jidonline.org, and at https://doi.org/10.1016/j.jid.2021.02.759.

REFERENCES

Agham SA, Sandip M, Savaliya D, Juneja AM. Sublingual route of drug delivery system: a review. PharmTechMedica 2012;1:22–30.

Akamatsu H, Komura J, Asada Y, Niwa Y. Mechanism of anti-inflammatory action of glycyrrhizin: effect on neutrophil functions including reactive oxygen species generation. Planta Med 1991;57:119–21.

Akdis M, Trautmann A, Blaser K, Akdis CA. T cells and effector mechanisms in the pathogenesis of atopic dermatitis. Curr Allergy Asthma Rep 2002;2:1–3.

Altin JG, Sloan EK. The role of CD45 and CD45-associated molecules in T cell activation. Immunol Cell Biol 1997;75:430–45.

Bandyopadhyay D, Kusari A, Kenner KA, Liu F, Chernoff J, Gustafson TA, et al. Protein-tyrosine phosphatase 1B complexes with the insulin receptor in vivo and is tyrosine-phosphorylated in the presence of insulin. J Biol Chem 1997;272:1639–45.

Brandt EB, Sivaprasad U. Th2 cytokines and atopic dermatitis. J Clin Cell Immunol 2011;2:110.

Choi JK, Oh HM, Lee S, Park JW, Khang D, Lee SW, et al. Oleanolic acid acetate inhibits atopic dermatitis and allergic contact dermatitis in a murine model. Toxicol Appl Pharmacol 2013;269:72–80.

Clark MA, Blair H, Liang L, Brey RN, Brayden D, Hirst BH. Targeting polymerised liposome vaccine carriers to intestinal M cells. Vaccine 2001;20:208–17.

Eichhorst ST, Krueger A, Müerköster S, Fas SC, Golks A, Gruetzner U, et al. Suramin inhibits death receptor–induced apoptosis in vitro and fulminant apoptotic liver damage in mice. Nat Med 2004;10:602–9.

Flint AJ, Gebbink MF, Franza BR, Hill DE, Tonks NK. Multi-site phosphorylation of the protein tyrosine phosphatase, PTP1B: identification of cell cycle regulated and phorbol ester stimulated sites of phosphorylation. EMBO J 1993;12:1937–46.

Fu B, Li H, Wang X, Lee FSC, Cui S. Isolation and identification of flavonoids in licorice and a study of their inhibitory effects on tyrosinase. J Agric Food Chem 2005;53:7408–14.

Fukai T, Marumo A, Kaitou K, Kanda T, Terada S, Nomura T. Anti-Helicobacter pylori flavonoids from licorice extract. Life Sci 2002;71:1449–63.

Gfeller D, Grosdidier A, Wirth M, Daina A, Michielin O, Zoete V. SwissTargetPrediction: a web server for target prediction of bioactive small molecules. Nucleic Acids Res 2014;42:W32–8.

Grammatikos AP. The genetic and environmental basis of atopic diseases. Ann Med 2008;40:482–95.

Hatano T, Kusuda M, Inada K, Ogawa TO, Shiota S, Tsuchiya T, et al. Effects of tannins and related polyphenols on methicillin-resistant Staphylococcus aureus. Phytochemistry 2005;66:2047–55.

He RJ, Yu ZH, Zhang RY, Zhang ZY. Protein tyrosine phosphatases as potential therapeutic targets. Acta Pharmacol Sin 2014;35:1227–46.

Johnson KG, Bromley SK, Dustin ML, Thomas ML. A supramolecular basis for CD45 tyrosine phosphatase regulation in sustained T cell activation. Proc Natl Acad Sci USA 2000;97:10138–43.

Kim YW, Zhao RJ, Park SJ, Lee JR, Cho IJ, Yang CH, et al. Anti-inflammatory effects of liquiritigenin as a consequence of the inhibition of NF-kappaB-dependent iNOS and proinflammatory cytokines production. Br J Pharmacol 2008;154:165–73.

Krishnan N, Krishnan K, Connors CR, Choy MS, Page R, Peti W, et al. PTP1B inhibition suggests a therapeutic strategy for Rett syndrome. J Clin Invest 2015;125:3163–77.

La VD, Tanabe S, Bergeron C, Gafner S, Grenier D. Modulation of matrix metalloproteinase and cytokine production by licorice isolates licoricidin and licorisoflavan A: potential therapeutic approach for periodontitis. J Periodontol 2011;82:122–8.

Lee HS, Choi EJ, Choi H, Lee KS, Kim HR, Na BR, et al. Oral administration of 4-hydroxy-3-methoxycinnamaldehyde attenuates atopic dermatitis by inhibiting T cell and keratinocyte activation. PLoS One 2015;10:e0144521.

Lee HS, Choi EJ, Lee KS, Kim HR, Na BR, Kwon MS, et al. Oral administration of p-hydroxycinnamic acid attenuates atopic dermatitis by downregulating Th1 and Th2 cytokine production and keratinocyte activation. PLoS One 2016;11:e0150952.

Leung DY, Bieber T. Atopic dermatitis. Lancet 2003;361:151–60.

Liu FT, Goodarzi H, Chen HY. IgE, mast cells, and eosinophils in atopic dermatitis. Clin Rev Allergy Immunol 2011;41:298–310.

Martin-Granados C, Prescott AR, Le Sommer S, Klaska IP, Yu T, Muckersie E, et al. A key role for PTP1B in dendritic cell maturation, migration, and T cell activation. J Mol Cell Biol 2015;7:517–28.

Mertins P, Eberl HC, Renkawitz J, Olsen JV, Tremblay ML, Mann M, et al. Investigation of protein-tyrosine phosphatase 1B function by quantitative proteomics. Mol Cell Proteomics 2008;7:1763–77.

Mustelin T, Coggeshall KM, Altman A. Rapid activation of the T-cell tyrosine protein kinase pp56lck by the CD45 phosphotyrosine phosphatase. Proc Natl Acad Sci USA 1989;86:6302–6.

Oyoshi MK, He R, Kumar L, Yoon J, Geha RS. Cellular and molecular mechanisms in atopic dermatitis. Adv Immunol 2009;102:135–226.

Ravichandran LV, Chen H, Li Y, Quon MJ. Phosphorylation of PTP1B at Ser(50) by Akt impairs its ability to dephosphorylate the insulin receptor. Mol Endocrinol 2001;15:1768–80.

Santamaria Babi LF, Picker LJ, Perez Soler MT, Drzimalla K, Flohr P, Blaser K, et al. Circulating allergen-reactive T cells from patients with atopic dermatitis and allergic contact dermatitis express the skin-selective homing receptor, the cutaneous lymphocyte-associated antigen. J Exp Med 1995;181:1935–40.

Seo CS, Lee JA, Jung D, Lee HY, Lee JK, Ha H, et al. Simultaneous determination of liquiritin, hesperidin, and glycyrrhizin by HPLC-photodiode array detection and the anti-inflammatory effect of Pyungwi-san. Arch Pharm Res 2011;34:203–10.

Shifrin VI, Davis RJ, Neel BG. Phosphorylation of protein-tyrosine phosphatase PTP-1B on identical sites suggests activation of a common signaling pathway during mitosis and stress response in mammalian cells. J Biol Chem 1997;272:2957–62.

Tanabe S, Desjardins J, Bergeron C, Gafner S, Villinski JR, Grenier D. Reduction of bacterial volatile sulfur compound production by licoricidin and licorisoflavan A from licorice. J Breath Res 2012;6:016006.

Yip SC, Saha S, Chernoff J. PTP1B: a double agent in metabolism and oncogenesis. Trends Biochem Sci 2010;35:442–9.

Zhang J, Gao W, Yan S, Zhao Y. Effects of space flight on the chemical constituents and anti-inflammatory activity of licorice (Glycyrrhiza uralensis Fisch). Iran J Pharm Res 2012;11:601–9.

Zhang ZY, Lee SY. PTP1B inhibitors as potential therapeutics in the treatment of type 2 diabetes and obesity. Expert Opin Investig Drugs 2003;12:223–33.

SUPPLEMENTARY MATERIALS AND METHODS

RT-PCR and real-time quantitative RT-PCR

Total RNA was isolated using TRIzol reagent (Thermo Fisher Scientific, Waltham, MA). Reverse transcription of the RNA was performed using RT PreMix (Enzynomics, Daejeon, Korea). The primers used for each gene were as follows (forward and reverse primers, respectively): human *IL-2*, 5′-CAC GTC TTG CAC TTG TCA C-3′ and 5′-CCT TCT TGG GCA TGT AAA ACT-3′; human *GAPDH*, 5′-CGG AGT CAA CGG ATT TGG TCG TAT-3′ and 5′-AGC CTT CTC CAT GGT GAA GAC-3′; mouse *Il-4*, 5′-ACA GGA GAA GGG ACG CCA t-3′ and 5′-GAA GCC GTA CAG ACG AGC TCA-3′; mouse *Il-5*, 5′-GAA GTG TGG CGA GGA GAG AC−3′ and 5′-GCA CAG TTT TGT GGG GTT TT−3′; mouse *Il-6*, 5′-CCG GAG AGG AGA CTT CAC AG−3′ and 5′-GGA AAT TGG GGT AGG AAG GA−3′; mouse *Il-13*, 5′-GCA ACA TCA ACA GGA CCA GA−3′ and 5′-GTC AGG GAA TCC AGG GCT AC−3′; mouse *Gata3*, 5′−CTC GGC CAT TCG TAC ATG GAA−3′ and 5′−GGA TAC CTC TGC ACC GTA GC−3′; and mouse *Gapdh*, 5′−GCA CAG TCA AGG CCG AGA AT−3′ and 5′−GCC TTC TCC ATG GTG GTG AA−3′. The PCR conditions were as follows: denaturation at 94 °C for 30 seconds, annealing at 60 °C for 20 seconds, and extension at 72 °C for 40 seconds. The 30 cycles were preceded by denaturation at 72 °C for 7 minutes. The expression levels of *IL-2* mRNA from Jurkat cells and mRNAs for inflammatory cytokines from ear tissues were evaluated by real-time RT-PCR. Total RNA was isolated, and cDNA was synthesized as described earlier. PCR amplification was performed in DNA Engine Opticon 1 continuous fluorescence detection system (MJ Research, Waltham, MA) using SYBR Premix Ex Taq (Takara, Kyoto, Japan). The total reaction volume was 10 μl, and it contained 1 μl of cDNA/control and gene-specific primers. Each PCR reaction was performed using the following conditions: 94 °C for 30 seconds, 60 °C 30 seconds, 72 °C for 30 seconds, and plate read (detection of fluorescent product) for 40 cycles followed by 7 minutes of extension at 72 °C. Melting curve analysis was performed to characterize the double-stranded DNA product by slowly raising the temperature (0.2 °C per second) from 65 °C to 95 °C with fluorescence data collected at 0.2 °C intervals. The levels of *IL-2* and cytokines mRNA normalized to *GAPDH* were expressed as fold changes relative to that of the untreated controls. The fold change in gene expression was calculated using the following equation: fold change $= 2^{-\Delta\Delta CT}$, where $\Delta\Delta CT$ = (CT Target−CT GAPDH) at time x−(CT Target−CT GAPDH) at time 0. In this equation, time x represents any time point, and time 0 represents the 1 × expression of the target gene in the untreated cells, normalized to *GAPDH*. All experiments were performed at least three times unless otherwise indicated.

MTT assay

Cell viability was determined using the MTT assay. Jurkat T cells (5×10^5) were incubated with the indicated concentration of licoricidin for 24 hours at 37 °C. Cells were then treated with MTT (500 μg/ml) for 2 hours. Subsequently, cell culture plates were centrifuged, the supernatant was discarded, and 200 μl of DMSO was added to each well to dissolve the formazan crystals. The plates were read at 540 nm, and the absorbance of each sample was calculated, relative to that of the control, and expressed as a percentage (% of the control).

Cell death assay using AnnexinV and 7-aminoactinomycin D

Cell death of Jurkat T cells was examined by a double staining method using AnnexinV conjugated with phycoerythrin and 7-aminoactinomycin D. Briefly, Jurkat T cells (5×10^5) were resuspended in 100 μl binding buffer (10 mM 4-[2-hydroxyethyl]-1-piperazineethanesulfonic acid, 150 mM sodium chloride, 5 mM potassium chloride, 5 mM magnesium chloride, and 1.8 mM calcium chloride) containing AnnexinV (20 μg/ml) and 7-aminoactinomycin D (1 μg/ml) and were incubated for 15 minutes at room temperature. The cells were then analyzed on a FACSCanto II (BD Biosciences, Franklin Lakes, NJ). Flowjo software was used for data analysis.

DAPI and phalloidin staining

Jurkat T cells (5×10^5) were treated with licoricidin (0–80 μM) for 24 hours and immobilized for 20 minutes at 37 °C onto coverslips coated with poly-L-lysine. The cells were then fixed in 2% paraformaldehyde for 30 minutes at room temperature and stained with tetramethylrhodamine B isothiocyanate phalloidin for 30 minutes at room temperature. Subsequently, the slides were washed with PBS, incubated for 3 minutes in PBS containing DAPI (500 ng/ml) at room temperature, and examined under a confocal microscope equipped with a DAPI filter.

Western blotting

Cells were homogenized in a lysis buffer (1% Triton X-100, 150 mM sodium chloride, 20 mM Tris pH7.5, 1 tablet of a protease inhibitor, and 1 tablet of phosphatase inhibitor) for 30 minutes on ice and centrifuged at 14,000 r.p.m. for 20 minutes at 4 °C. Approximately 50 μg of the extract lysate was separated on 8–12% SDS−PAGE gels. Proteins were transferred onto a nylon membrane using the Trans-Blot SD semi-dry transfer cell (Bio-Rad, Hercules, CA). The membrane was blocked in 5% skim milk (for 1 hour), rinsed, and incubated with the indicated primary antibodies in Tris-buffered saline containing 0.1% Tween 20 and 3% skim milk overnight. Excess primary antibodies were removed by washing the membrane four times in Tris-buffered saline containing 0.1% Tween 20. The membrane was then incubated with 0.1 μg/ml peroxidase–labeled secondary antibodies (against rabbit or mouse) for 1 hour. After three washes in Tris-buffered saline containing 0.1% Tween 20, bands were visualized using ECL Western Blotting Detection Reagents (iNtRON Biotechnology, Seongnam, Korea).

Tyrosine-protein phosphatase nonreceptor type 1 activity assay

For tyrosine-protein phosphatase nonreceptor type 1 activity assay, tyrosine-protein phosphatase nonreceptor type 1 colorimetric assay kit (BPS bioscience, San Diego, CA) was used according to the manufacturer's instructions.

Proliferation assay

Pretreated Jurkat T cells with the indicated concentration of licoricidin were stained with 1 μM carboxyfluorescein succinimidyl ester and stimulated with anti-CD3 (20 μg/ml)/

CD28 (7 μg/ml) antibodies for 24 hours. After stimulation, histogram shift was acquired by flow cytometry.

Measurement of AnnexinV and caspases 3 and 7 by IncuCyte

Treated cells with the indicated conditions were stained with 1 μM of AnnexinV, and caspases 3 and 7 reagents were added to the cells. Microscopic images with green (AnnexinV) and red (caspases 3 and 7) fluorescences were acquired by IncuCyte imaging system, and intensities were integrated by IncuCyte software. All intensities were normalized with an intensity of control and presented in a bar graph.

T-cell differentiation

T-cell differentiation assay was performed as previously reported (Lee et al. 2016). Briefly, isolated $CD4^+$ mouse T cells were incubated with immobilized anti-CD3 (2 μg/ml) coated plates and soluble anti-CD28 (2 μg/ml). For T helper type 1 differentiation, cells were incubated with anti–IL-4 antibody (10 μg/ml), IL-12 recombinant protein (10 ng/ml), and IL-2 recombinant protein (2 IU). For T helper type 2 differentiation, cells were incubated with anti–IFN-γ antibody (5 μg/ml), anti–IL-12 antibody (5 μg/ml), IL-4 recombinant protein (10 ng/ml), and IL-2 recombinant protein (2 IU). After 5 days of incubation, differentiated cells were harvested for isolation of total RNA to determine the expression of Tbet (T helper type 1) and GATA3 (T helper type 2).

ELISA

For IgE measurement, the blood samples were collected, and plasma or serum was prepared by centrifugation. The amounts of total IgE, mite-specific IgE, IgG1, and IgG2a were determined by a commercial ELISA kit according to the manufacturer's instructions. For mouse IL-2 measurement, supernatants were harvested, and the produced mouse IL-2s were measured by DuoSet ELISA kit (R&D Systems, Minneapolis, MN).

Knockdown with small interfering RNA transfection

For knockdown experiments, transient transfection of Jurkat cells with small interfering RNA targeting human tyrosine-protein phosphatase nonreceptor type 1 was performed using Amaxa Nucleofector kits (Lonza, Basel, Switzerland) according to the manufacturer's instructions.

SUPPLEMENTARY REFERENCE

Lee HS, Choi EJ, Lee KS, Kim HR, Na BR, Kwon MS, et al. Oral administration of p-hydroxycinnamic acid attenuates atopic dermatitis by downregulating Th1 and Th2 cytokine production and keratinocyte activation. PLoS One 2016;11:e0150952.

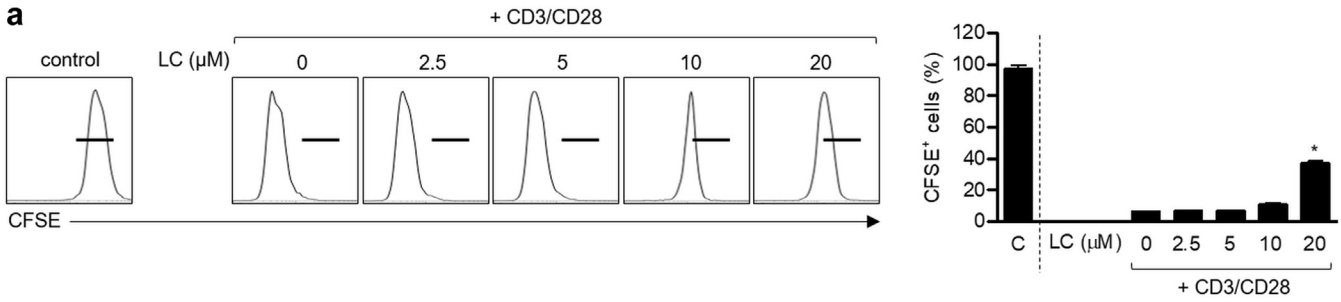

Supplementary Figure S1. Licoricidin reduces T-cell proliferation in the presence of TCR-mediated stimulation. Pretreated Jurkat T cells with 0–20 μM were stained with 1 μM CFSE and stimulated with anti-CD3/-CD28 antibodies for 24 hours. After stimulation, cells were acquired by flow cytometry. CFSE-positive cells are presented in a bar graph. Results are expressed as mean ± SEM of three independent experiments. *$P < 0.05$. C, control; CFSE, carboxyfluorescein succinimidyl ester.

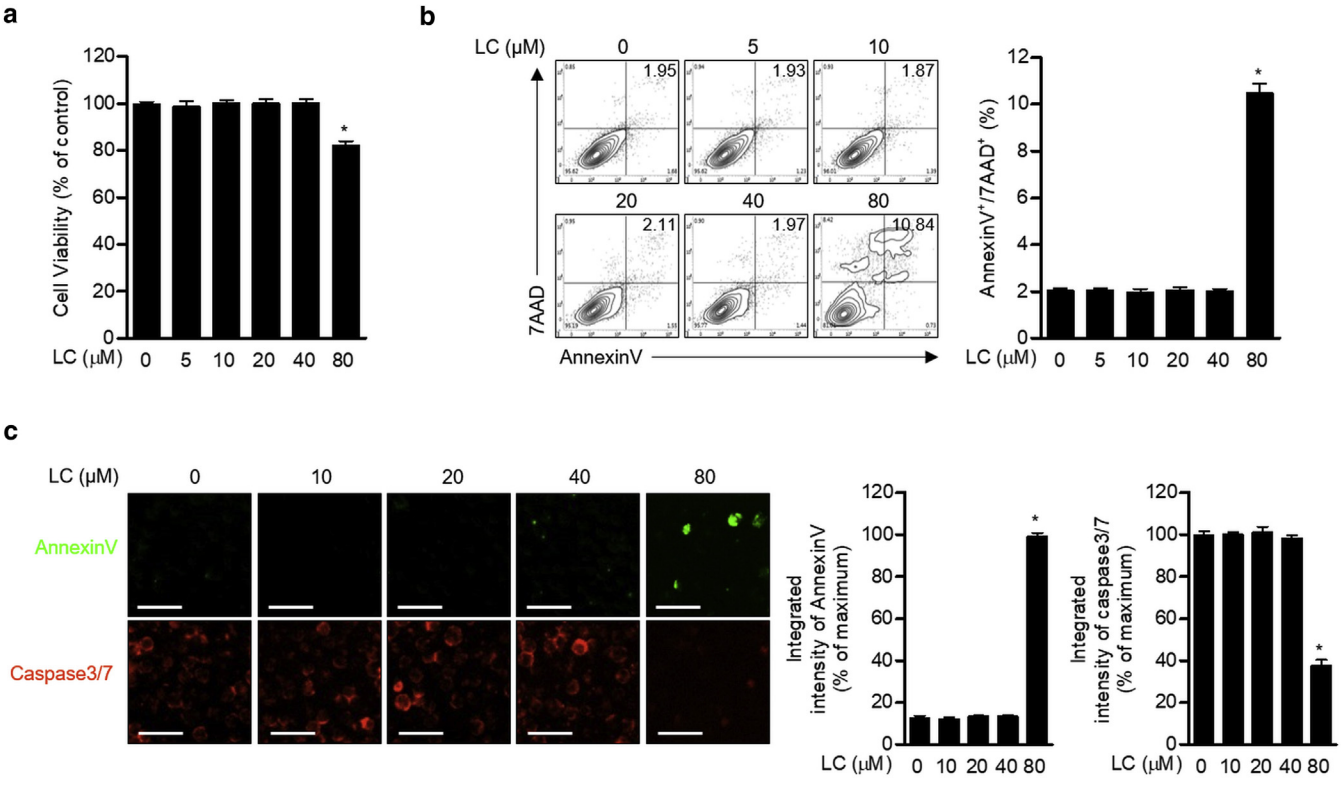

Supplementary Figure S2. LC does not show cytotoxic effects in mouse CD4$^+$ primary T cells. (**a**) Cell viability was assessed by MTT after incubation of LC (0–80 μM). (**b**) After incubation of LC (0–80 μM), apoptosis assay using AnnexinV and 7-AAD was performed. AnnexinV$^+$/PI$^+$ population is presented in a bar graph. (**c**) The expressions of AnnexinV and caspase3/7 were assessed by IncuCyte imaging system from cells treated with LC (0–80 μM). The integrated intensities are presented in a bar graph. Results are expressed as mean ± SEM of three independent experiments. *$P < 0.05$. Bar = 50 μm. 7-AAD, 7-aminoactinomycin D; LC, licoricidin; PI, propidium iodide.

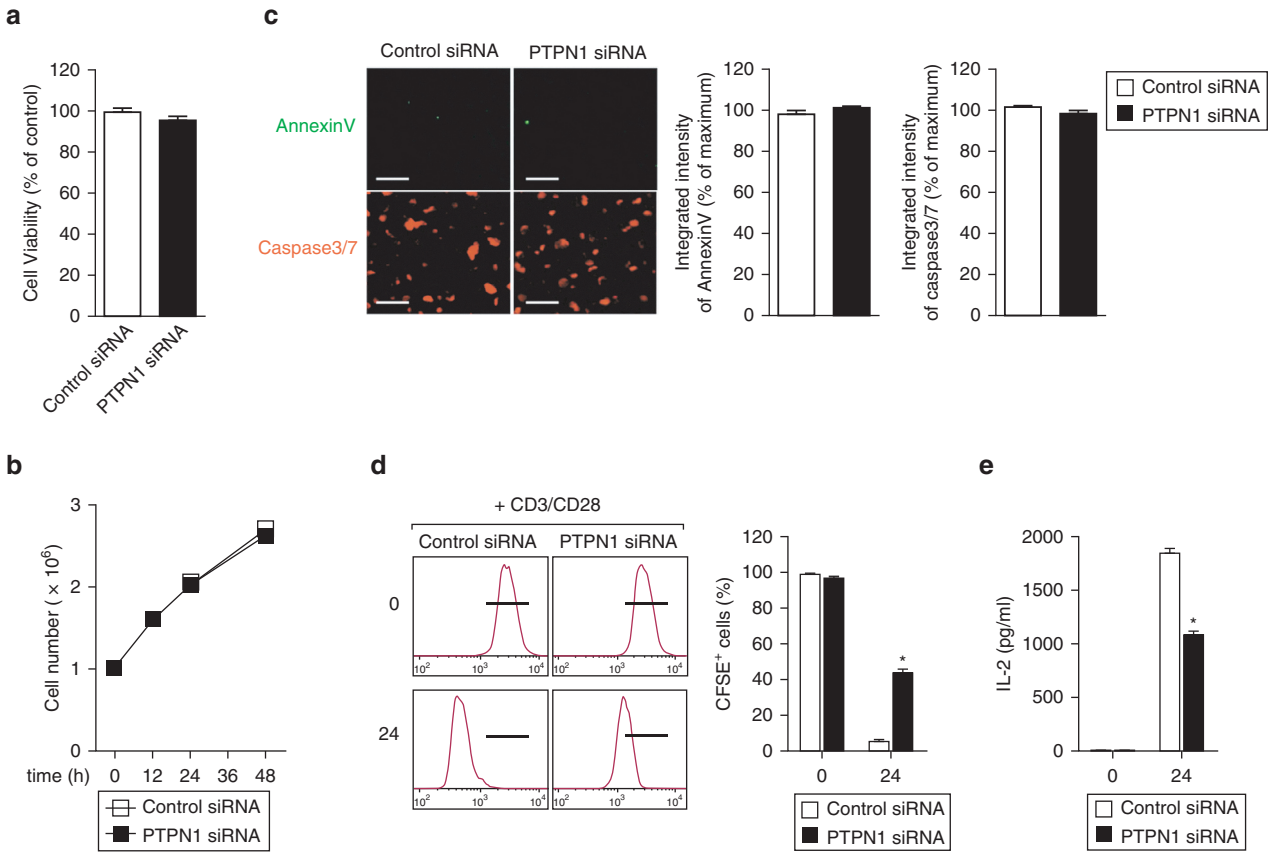

Supplementary Figure S3. PTPN1 deficiency is not cytotoxic in Jurkat T cells. (**a**) Cell viability was assessed by MTT after 24 h of transfection with siRNAs (control and PTPN1). (**b**) Cell growth rate was obtained by counting the cell numbers of each group every 12 h. (**c**) The expressions of AnnexinV and caspase3/7 were assessed by IncuCyte imaging system from cells transfected with siRNAs (control and PTPN1). Integrated intensities are presented in a bar graph. (**d**) Jurkat T cells transfected with control or PTPN1 siRNA were stained with 1 μM CFSE for 30 minutes and stimulated with anti-CD3m/-CD28 antibodies for 24 h. Cells were harvested, and the proliferation of T cells was assessed by flow cytometry. (**e**) After stimulation, supernatants were collected, and the produced IL-2s were measured by ELISA. Bar = 50 μm. CFSE, carboxyfluorescein succinimidyl ester; h, hour; PTPN1, tyrosine-protein phosphatase nonreceptor type 1; siRNA, small interfering RNA.

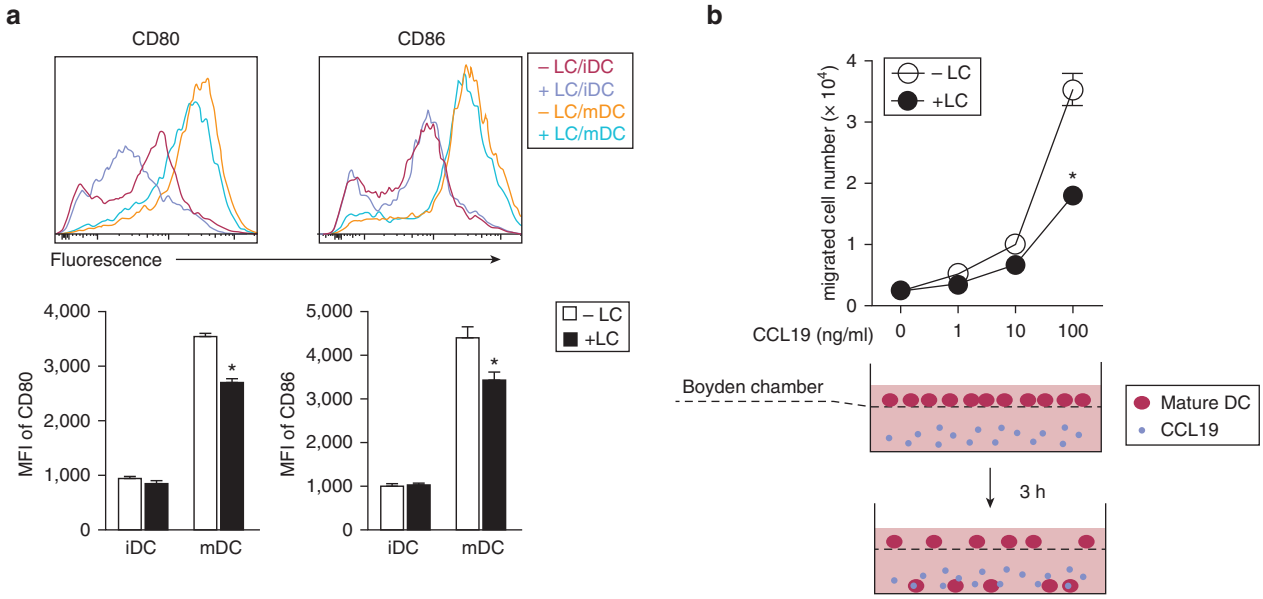

Supplementary Figure S4. Treatment with licoricidin reduces DC maturation and migrating capacity toward CCL19. (**a**) After differentiation into BMDCs from bone marrow cells for 6 days; cells were treated with LPS (1 μg/ml) for 24 h in the presence or absence of licoricidin (20 μM). Mean fluorescence intensities of CD80 and CD86 were measured by flow cytometry from iDCs and mDC. (**b**) Stained mDC (1×10^5) with CMFDA green cell tracker were loaded on Boyden chamber (5-μm pore size), which contained the indicated concentration of CCL19 in the bottom wells. After 3 h of incubation at 37 °C, migrating cells in the bottom wells were harvested, and the number of cells was counted by flow cytometry. Results are expressed as mean ± SEM of three independent experiments. *$P < 0.05$. BMDC, bone marrow–derived dendritic cell; CMFDA, 5-chloromethylfluorescein diacetate; DC, dendritic cell; h, hour; iDC, immature dendritic cell; LPS, lipopolysaccharide; mDC, mature dendritic cell; MFI, mean fluorescence intensity.

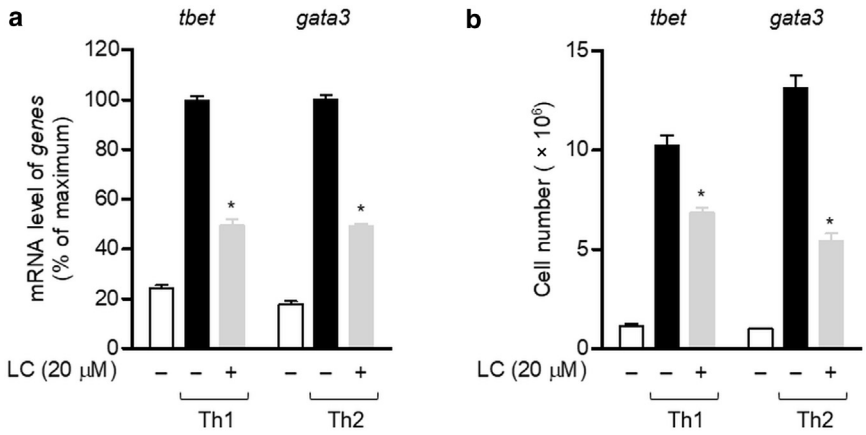

Supplementary Figure S5. Licoricidin inhibits T-cell differentiation into Th1 and Th2. (**a**) mRNA levels of *TBET* and *GATA3* were measured by qPCR from polarized T cells into Th1 and Th2, respectively. Licoricidin (20 μM) was added to the initial step of differentiation. (**b**) Cell number was counted every day from each group during differentiation for 5 days. Results are expressed as mean ± SEM of three independent experiments. *$P < 0.05$. Th, T helper.

Supplementary Table S1. List of the Predicted Targets of Licoricidin by Swiss TargetPrediction Website

Target	Common Name	Uniprot ID
Tyrosinase	TYR	P14679
Protein-tyrosine phosphatase 1B	PTPN1	P18031
Arachidonate 15-lipoxygenase, type II	ALOX15B	O15296
Pyruvate dehydrogenase kinase isoform 1	PDK1	Q15118

Abbreviation: SMILES, simplified molecular-input line-entry system.

The target protein of licoricidin was predicted by the Swiss TargetPrediction website. The following canonical SMILES code was used for search: CC(=CCC1=C(C=CC(=C1O)C2CC3 =C(C(=C(C=C3OC2)O)CC=C(C)C)OC)O)C. Probabilities were computed on the basis of cross validation. Candidate proteins were cut off by probabilities, and 3 candidates were shown at July, 2021.